Single-molecule imaging of cytoplasmic dynein in vivo

Vaishnavi Ananthanarayanan*[,1]**, Iva M. Tolić***[,§]

**Max Planck Institute of Molecular Cell Biology and Genetics, Dresden, Germany*
§*Division of Molecular Biology, Ruđer Bošković Institute, Zagreb, Croatia*
[1]*Current affiliation: Bioengineering Programme, Indian Institute of Science, Bangalore, India*
Corresponding author: E-mail: vaish@be.iisc.ernet.in

CHAPTER OUTLINE

Abstract

While early fluorescence microscopy experiments employing fluorescent probes afforded snapshots of the cell, the power of live-cell microscopy is required to understand complex dynamics in biological processes. The first successful cloning of green fluorescent protein in the 1990s paved the way for development of approaches that we now utilize for visualization in a living cell. In this chapter, we discuss a technique to observe fluorescently tagged single

molecules in fission yeast. With a few simple modifications to the established total internal reflection fluorescence microscopy, cytoplasmic dynein molecules in the cytoplasm and on the microtubules can be visualized and their intracellular dynamics can be studied. We illustrate a technique to study motor behavior, which is not apparent in conventional ensemble studies of motors. In general, this technique can be employed to study single-molecule dynamics of fluorescently tagged proteins in the cell interior.

INTRODUCTION

Motor proteins are molecular machines responsible for processes ranging from cellular and muscle contractility to transport and positioning of cellular cargo (Sellers, 2000; Vale, 2003). Kinesins and cytoplasmic dynein (referred to as "dynein" from here on) are the motors that ferry materials across the cell using microtubules (MTs) as tracks, with kinesins typically moving toward the plus ends of MTs and dyneins moving in the opposite direction, toward the minus ends of MTs. Motor behavior has been studied in the past using a variety of in vivo and in vitro techniques. Specifically, single-molecule quantification of motor force production, stepping, and directionality has been performed using optical tweezers (Block, Goldstein & Schnapp, 1990; Gennerich & Reck-Peterson, 2011; Kuo & Sheetz, 1993; Reck-Peterson, Yildiz, Carter, Gennerich, Zhang & Vale, 2006; Svoboda, Schmidt, Schnapp, & Block, 1993). The interactions between purified motors and MTs have also been investigated using light microscopy techniques such as Total Internal Reflection Fluorescence Microscopy (TIRFM) in conventional MT gliding and motor stepping assays (Korten, Nitzsche, Gell, Ruhnow, Leduc & Diez, 2011; Vale, Funatsu, Pierce, Romberg, Harada & Yanagida, 1996; Vale, Schnapp, Reese, & Sheetz, 1985). These in vitro techniques offer the advantage of selective addition or exclusion of motor interactors to assay their effect on motor properties. However, to understand how the motor protein works in a live cell, it is essential that the study is conducted in a cellular environment, in the presence of its various regulators. In an in vivo setting, light microscopy has largely been restricted to observation of ensemble motor properties, which can yield qualitative information about the motor function, but not single-motor properties. However, with the improvement of microscopy techniques, the detection of single molecules in live cells is becoming increasingly possible (see also Leduc et al. and Yamashiro et al. REFS in the same volume). In this chapter, we will see how we can utilize the power of fluorescence light microscopy to study single-molecule behavior of the motor protein dynein in vivo (Ananthanarayanan, Schattat, Krull, Vogel, Pavin & Tolić-Nørrelykke, 2013).

1. VISUALIZATION OF CYTOPLASMIC DYNEIN IN VIVO
1.1 BACKGROUND

The technique presented in this chapter for visualization of single motors can be applied to several systems—to study myosin motors during cortical flows, kinesin and dynein dynamics during endocytosis, and cell division, to name a few. Here,

as proof-of-principle, we focus on the fission yeast nuclear oscillations system that employs the motor protein dynein.

In fission yeast, the motor protein dynein, which is anchored at the cortex, is required for powering the oscillations of the fused zygotic nucleus from one cell pole to the other (Yamamoto, West, McIntosh & Hiraoka, 1999). Nuclear oscillations in fission yeast are essential for ensuring proper chromosome pairing and recombination (Yamamoto, Tsutsumi, Kojima, Oiwa, & Hiraoka, 2001). Dynein in the zygote could be (1) freely diffusing in the cytoplasm, (2) bound to the MT, or (3) bound simultaneously to the MT and the anchor protein at the cortex (Saito, Okuzaki, & Nojima, 2006; Vogel, Pavin, Maghelli, Julicher, & Tolić-Nørrelykke, 2009; Yamamoto et al., 2001; Yamashita & Yamamoto, 2006). To study these three populations of dynein at a single-molecule level, a high signal-to-noise ratio (SNR) is required. TIRFM offers this high SNR by selectively illuminating the sample up to a depth of 100–200 nm from the surface of the coverslip (Axelrod, 1981; Coelho, Maghelli & Tolić-Nørrelykke, 2013; Iino, Koyama & Kusumi, 2001; Reck-Peterson, Derr & Stuurman, 2010), which is useful for imaging cell membrane-restricted proteins. But for visualization of the freely moving population of dynein in the cytoplasm or the MT-bound dynein population, a higher penetration depth is required, approaching close to half the cell depth of a 4-μm-deep fission yeast zygote. Hence, a variation of TIRFM, called Highly Inclined and Laminated Optical Sheet (HILO) Microscopy, is used to achieve a high penetration depth, but retain the advantage of high SNR, by illuminating with a sheet of light (Tokunaga, Imamoto & Sakata-Sogawa, 2008). Any conventional TIRFM setup can be adapted for HILO with a high inclination of the incident laser at the coverslip–sample interface to induce a large refraction of the light within the sample (Figure 1).

1.2 EXPERIMENT

The fission yeast system is an excellent model for this imaging technique because of its small size, the presence of few MTs, and low protein copy number. While it is good to have similar characteristics in other systems to be able to employ this experiment, a few changes to the experimental and imaging protocols can circumvent many shortcomings. For example, in a system overexpressing the fluorescent protein of interest, or one with a dense MT network, prebleaching (see *Observation of Dyneins on the microtubule* below) alleviates the inherently low SNR. In mammalian cells, transfecting cells with bacterial artificial chromosomes to express a fluorescent protein of interest, instead of a conventional expression vector, can also result in lower number of signal-producing molecules and hence, higher resolution in imaging.

1.2.1 *Preparation of fission yeast zygotes*

For single-molecule observation of dynein in fission yeast, a strain with the dynein heavy chain (Dhc1) labeled with GFP (green fluorescent protein) or 3GFP is used (Vogel et al., 2009; Yamamoto et al., 1999). The heavy chain of dynein is the largest moiety of dynein that contains the ATP-binding and hydrolysis sites at the
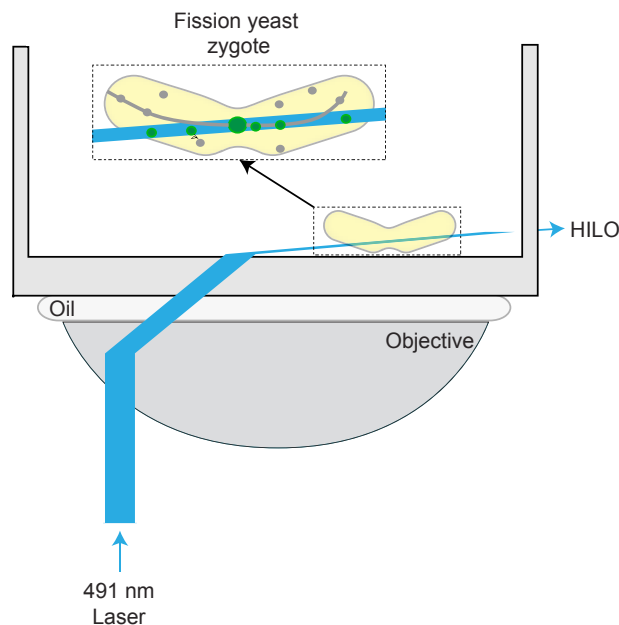
FIGURE 1

Highly Inclined and Laminated Optical Sheet (HILO) imaging of dyneins in a living fission yeast zygote. Scheme of the light path during HILO imaging of a fission yeast zygote in which the dynein is tagged with GFP. The laser light sheet (blue) from HILO imaging passes at a certain depth into the cell, specifically illuminating only those dyneins in its path (green), resulting in a high signal-to-noise ratio. Dyneins which do not fall under this sheet of light (gray) do not fluoresce. (See color plate)

C-terminus, as well as dimerization sites at the N-terminal tail domain (Kardon & Vale, 2009). Thus, a complete dynein complex in this strain contains a homodimer of heavy chains, each labeled with a single GFP or 3GFP. Meiosis is induced with nitrogen starvation of cells (see Methods below). Most zygotes are in the meiotic prophase 7—8 h post meiosis induction, when the nuclear oscillations occur.

1.2.2 Observation of dyneins in the cytoplasm

Dyneins in the cytoplasm are free molecules and hence are expected to exhibit Brownian movement. This thermally induced movement of dynein in the cytoplasm is orders of magnitude faster than the movement of bound dyneins on the MT. As a result, the time resolution of imaging dyneins in the cytoplasm needs to be higher than that of dyneins bound to MTs. Further, the density of dyneins on a given MT is higher than in the cytoplasm, making it difficult to resolve individual molecules on the MT. To solve this problem, we employ prebleaching (see *Observation of Dyneins on the microtubule* below). We will first set up the TIRFM system for

imaging dyneins in the cytoplasm and then change a few parameters to adapt the same system for visualizing dyneins bound to the MT.

A 491-nm laser line is first calibrated for TIRFM on a wide-field microscope fitted with an Olympus iXon EMCCD detector. Following this, the dish containing the zygotes is introduced into the dish holder. Zygotes are identified by their characteristic shape and the camera is then employed to observe fluorescence of GFP under 491-nm laser illumination. Initially, a low laser power of about 1.125 mW (5% setting) is used to verify that the cell is indeed in the nuclear oscillations phase. In the live mode, the knob for controlling laser illumination angle is progressively turned so as to be able to observe dynein fluorescence from the spindle pole body (SPB, centrosome equivalent in yeast), from a portion of the MT bound by dyneins and from the cytoplasm of the zygote. In systems where the laser angle is controlled via the software, a suitable angle is chosen to obtain the same result. Further focusing, using the focusing knobs, of the microscope is done if necessary. Essentially, in this step, we are transitioning from the TIRF mode to the HILO mode. The region of interest (ROI) of imaging is cropped to include only the cell of interest. This considerably reduces image acquisition and transfer time and thus increases the time resolution of imaging. The laser power is then increased to about 18 mW (80% setting), the imaging protocol is set to acquire 2000 frames in a stream with an exposure time of 5–9 ms for each frame, to get a net frame rate of close to 200 fps. Frame display is disabled during acquisition as this leads to decreased frame rates of imaging. An example of a movie thus acquired is depicted in Figure 2.

1.2.3 Observation of dyneins on the microtubule

For imaging dyneins that bind to the MT from the cytoplasm and to follow their movement while on the MT, the imaging dish with fission yeast zygotes is prepared as detailed above. Imaging in the HILO mode is set up so as to observe the SPB and MTs in focus in the plane of imaging. In most systems, it is unlikely that an entire MT bundle of interest is in the plane of imaging, and additional complication is brought about by dynamicity of the MT. However, single-molecule visualization of dynein is still possible with at least a portion of the MT visible during our imaging. Again, the ROI is restricted to the cell of interest. The cell is first prebleached with about 18-mW power of 491-nm laser, with an exposure time of ∼8 ms and repetition of 800 times. During this time, the signal emanating from dyneins on the MT in the plane of imaging is bleached. Following this prebleaching step, the binding of dyneins afresh from the cytoplasm can be observed, and their subsequent movement on the MT is followed by imaging with 18 mW of the 491 nm laser at 1 fps, by setting an exposure time of ∼5 s with an interval of 1 s between frames and with a repetition of 100 frames. An example of imaging of dyneins on the MT can be seen in Figure 3.

1.2.4 Discussion

1.2.4.1 Prebleaching to observe dyneins with higher SNR

From the example cells in Figure 2, we see that the photobleaching rate is high. In about 200 frames (∼1 s), the total fluorescence intensity is halved. As discussed
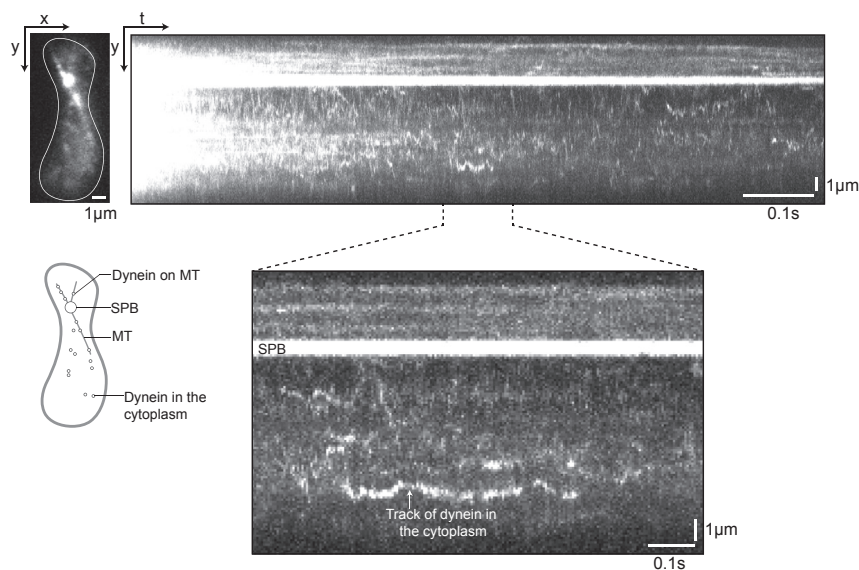
FIGURE 2

Visualization of dyneins in the cytoplasm. Highly Inclined and Laminated Optical Sheet (HILO) image (top left) and scheme (bottom left) of a fission yeast zygote expressing Dhc1-3GFP. The maximum intensity projection onto the y-axis has been shown on the top right. While dynein traces are hard to distinguish in the initial frames of the movie, in the later frames, where the dynein fluorescent signal emanating from the plane of imaging has bleached away, dynein traces are clearly visible. The dashed lines show an enlarged portion of the maximum intensity projection, with one such track of dynein in the cytoplasm.

earlier, in this experiment, this photobleaching is used to our advantage, since when we bleach the signal emanating from the focused plane of imaging, other unbleached, fluorescent dynein molecules arrive from the other unbleached planes and are observed as high SNR objects that can be clearly followed. Thus, in cases where the inherent SNR is low due to the high background caused by high density of the fluorescent proteins of interest, this prebleaching technique can be used to artificially increase the SNR. So too, when imaging dyneins on the MT as in Figure 3, the prebleaching step is required to follow dyneins that bind from the cytoplasm to the MT and thereupon, their movement on the MT can be tracked unambiguously due to the high SNR.

1.2.4.2 Estimation of penetration depth of HILO

Images obtained from our HILO system do not contain signal from the entire cell, but rather only a portion of it. Therefore for cell-wide quantification, one needs to be able to estimate the penetration depth in HILO imaging and then extrapolate parameters like number of molecules in the entire cell. For calculation of the penetration depth, simple geometry is employed, assuming circular cross-section of the cell
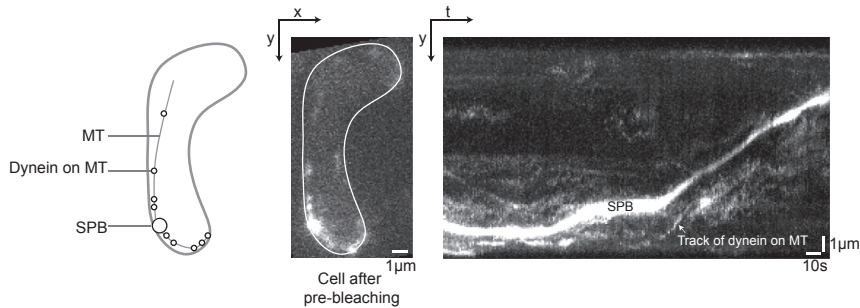
FIGURE 3

Visualization of dyneins on the microtubule. Scheme (left) and Highly Inclined and Laminated Optical Sheet (HILO) image after prebleaching (center) of a fission yeast zygote expressing Dhc1 tagged with GFP. Upon prebleaching, images are acquired at 1 fps to obtain the maximum intensity projection onto the y-axis (right). The tracks of the SPB and of a dynein molecule on the microtubule have been indicated.

at right angles to the long axis and to the surface of the coverslip. The width of the cell illuminated in HILO microscopy ($2l$) is compared to that from a z-projection of the entire cell acquired by spinning disk confocal microscopy ($2r$) (Figure 4).

The penetration depth d is then obtained by

$$d = r - \sqrt{(r^2 - l^2)}$$

In our HILO imaging, we estimated a penetration depth d of about 1.34 μm. This translates to about 1/3 the cell depth of a typical fission yeast zygote that has a depth of about 4 μm.

2. IMAGE ANALYSIS
2.1 TRACKING OF SINGLE MOLECULES

Tracking of fluorescent dynein molecules in the cytoplasm can be carried out using software packages such as u-track (Jaqaman, Loerke, Mettlen, Kuwata, Grinstein, Schmid, et al., 2008) or Low Light Tracking Tool (Krull, Steinborn, Ananthanarayanan, Ramunno-Johnson, Petersohn & Tolić-Nørrelykke, 2014). The Low Light Tracking Tool is especially suited for tracking dim objects in a high background setting, as is the case with observation of dynein molecules. The software is available for use as a Fiji plugin and more information on the usage of the software can be found at http://fiji.sc/Low_Light_Tracking_Tool.

In addition to position information in x and y with time, the Low Light Tracking Tool provides the background-subtracted intensity of each particle tracked. These data can then be used to confirm tracking of single molecules (see below) as well as to study the dynamics of movement of the particle.

FIGURE 4

Highly Inclined and Laminated Optical Sheet (HILO) penetration depth estimation. The penetration depth in our HILO imaging can be estimated from comparison of the cell widths of fission yeast zygotes in a z-projection of images from spinning disk (SD) confocal microscopy ($2r$, solid black line) and the images from HILO microscopy ($2l$, dashed magenta line (dashed line with arrow heads in print versions)), as explained in the text.

2.2 CONFIRMATION OF SINGLE-MOLECULE IMAGING

To confirm that the dyneins imaged are single molecules, multiple approaches may be used. In vitro, the most commonly employed technique is to observe bleaching steps of molecules (Ulbrich & Isacoff, 2007). The rationale behind this approach is that when fluorescently tagged molecules undergo photobleaching, the presence of multiple fluorophores on the molecules will be seen as discrete "steps" in the bleaching profile, with each step having the same "height," i.e., drop in fluorescence intensity. The total number of steps of bleaching thus observed until the signal from the molecule is equal to background corresponds to the number of fluorophores on the molecule or cluster of molecules. In the case of a dynein with its heavy chain tagged with GFP (Dhc1-GFP), for a single molecule, we would be able to observe two such steps of equal height, since the dynein complex consists of a homodimer of heavy chains and would thus have two GFP molecules. Software packages such as STEPFINDER (Kerssemakers, Munteanu, Laan, Noetzel, Janson & Dogterom, 2006) are available to automatically identify the bleaching steps for a given dataset. This method of identifying bleaching steps is useful when the molecule is at a constant depth of imaging for a sufficient time so as to visualize the intensity drop to background levels, such as a fluorescent motor walking on an MT track in vitro imaged using TIRF microscopy. However, in our HILO imaging, where the movement of dyneins in the cytoplasm is observed, the molecule is constantly moving from the plane of imaging to another plane or vice versa, leaving little time to observe photobleaching at the single-molecule level. Similarly, in the experiment of dyneins bound to the MT (Figure 3), dynein molecules typically do not stay on the MT long enough for us to be able to observe bleaching steps. Thus we modify the method of identifying bleaching steps to confirm observation of single molecules to observe clusters of dyneins on the MT in our fast movies. In the 200 fps movies which we employ for visualizing dyneins in the cytoplasm, we identify those molecules that are on the MT and hence stationary for the time period of the entire movie ($\sim$15 s). The bleaching profiles of these molecules are then obtained and subject to

analysis using the STEPFINDER software (Kerssemakers et al., 2006). The number of steps for each of the traces is greater than two, indicating the presence of more than one molecule of dynein at each of the spots chosen for tracing. However, the height of the final step across traces gives the intensity of a single GFP molecule and can be used as a reference (see Ananthanarayanan et al., 2013; Supplementary Figure S1D). The value thus obtained for single GFP intensity matches the value obtained from the analysis below, involving analysis of intensity histograms.

Alternatively, the number of dyneins in a tracked spot may be estimated from the distribution of dynein intensities. For the Dhc1-GFP strain, the intensities of all single-dynein molecules are expected to follow a distribution which is a mixture of two Gaussians, since there are at most two populations of visible dyneins in this strain—one with a single GFP intact (not bleached) and one with both GFPs intact. Indeed, we obtain a fit for the intensity data of GFP-labeled dynein in the cytoplasm as a mixture of two Gaussians, with the peak of the second Gaussian being twice as that of the first (see Ananthanarayanan et al., 2013; Supplementary Figure S1F). In addition, the mean of the first Gaussian, which gives the intensity of a single GFP in our imaging, is comparable to the intensity of the last step obtained in the bleaching step estimation above. Thus, we confirm that we are indeed visualizing single dyneins in the cytoplasm of fission yeast.

2.3 **ANALYSIS OF DYNEIN MOVEMENT**

The movement of fluorescently tagged dyneins in the cytoplasm and on the MTs is analyzed using mean squared displacement (MSD) analysis. For each time interval (Δt), the displacement of a single dynein molecule is calculated and squared. The mean of all such displacements gives the MSD data for that particular Δt for that single dynein molecule. For our analysis, we perform an ensemble nonoverlapping MSD for all dynein traces such that the squared displacement for all dynein traces for a given Δt is averaged to get the MSD. The time interval window is shifted across each dynein trace so as to have nonoverlapping, independent data points. The data thus obtained are plotted with time interval on the x-axis and MSD on the y-axis. The x-limit is chosen so as to be equal to half the average duration of all dynein traces. For example, if the average length of all dynein traces is 20 s, the x-limit is chosen to be a time interval of 10 s. This is done because for a trace with a length of 20 s, there will be only two data points for nonoverlapping squared displacement data for Δt of 10 s and for a Δt greater than 10 s for a 20-s long trace, there will be only one data point. Subsequently, the data are binned and a weighted fit to the equation $MSD = 2d \cdot D \cdot \Delta t + \text{offset}$ is performed, with weights being reciprocals of the number of data points in each bin, d being the dimension (equal to 2 for dynein tracked in the cytoplasm in two dimensions and equal to 1 for dynein tracked in one dimension on the MT), and D the diffusion coefficient. This equation is chosen since for simple diffusion, which is observed for dyneins in the cytoplasm and for those on the MT, the fit is linear. The bins with low Δt, which contain more data points, have higher weights. The diffusion coefficient (D) is then calculated from the slope of the fit. For

directed movement of a motor, a modified equation, $MSD = v^2 \cdot \Delta t^2 + 2D_{MT} \cdot \Delta t +$ offset is employed, where v is the velocity of movement and D_{MT}, diffusion on the MT.

3. CONCLUSION

In this chapter, we describe how single-molecule imaging of the motor protein dynein inside living cells can be carried out using HILO microscopy. This technique led us to the discovery of a mode of regulation of dynein behavior: dynein diffuses on the MT until it binds to its cortical anchor, whereupon it switches to directed movement (Ananthanarayanan et al., 2013). Visualization of single molecules using HILO microscopy may be extended to other model systems to study dynein and other MT-, actin-, or DNA-based motor proteins, or in general, the behavior of any fluorescently tagged proteins in the interior of living cells.

4. METHODS
4.1 CELL CULTURE

Cells are grown on Yeast Extract or Edinburgh Minimal Medium (EMM) (Forsburg & Rhind, 2006) with appropriate supplements at $25 \pm 0.5\ °C$ in a Heraeus incubator (Thermo Scientific, Waltham, MA, USA). Meiosis is induced by suspending a toothpickful of fresh cells in 50 μL of 0.85% sodium chloride (Merck KGaA, Darmstadt, Germany) and spotting onto Malt Extract Agar (MEA) plates. The plates are then incubated for 6−8 h at $25 \pm 0.5\ °C$.

4.2 PREPARATION OF SAMPLES FOR IMAGING

For imaging, a loopful of cells from the MEA plate is resuspended in 100 μL of EMM-N. The resuspended cells are transferred to a lectin-coated (L2380, Sigma-Aldrich, St Louis, MO, USA), 35-mm (No1.5) glass bottom culture dish (MatTek Corporation, Ashland, MA, USA) and allowed to stick to the glass for 5 min. The unbound cells are then washed out with EMM-N and live-cell imaging is performed at room temperature (22−25 °C).

4.3 MICROSCOPY

For HILO imaging, a custom-built TIRF condenser and manual TIRF angle adjustment unit on an inverted stand, manual XY stage Olympus IX71 microscope (Olympus, Tokyo, Japan) with an Olympus UApo 150x 1.45 Oil TIRFM inf/0.13−0.21 corr (Olympus, Tokyo, Japan) objective, and diode-pumped solid state 491 nm laser for GFP excitation (75 mW; Cobolt, Solna, Sweden) are employed. An acousto-optic tunable filter in the Andor Revolution laser combiner (ALC, Andor Technology plc., Belfast, UK) is used to control laser intensity and a BL HC 525/30

wavelength filter for GFP emission (Semrock Inc., Rochester, NY, USA). The detector is an Andor iXon EM + DU-897 BV back illuminated EMCCD (Andor Technology plc., Belfast, UK) with EMCCD chip pixel size of 16 μm and image pixel size of 0.106 μm with the 150x objective. The entire system is managed with the Andor iQ software version 1.9.1 (Andor Technology plc., Belfast, UK).

REFERENCES

Ananthanarayanan, V., Schattat, M., Vogel, S. K., Krull, A., Pavin, N., & Tolić-Nørrelykke, I. M. (2013). Dynein motion switches from diffusive to directed upon cortical anchoring. *Cell, 153*(7), 1526−1536. http://dx.doi.org/10.1016/j.cell.2013.05.020.

Axelrod, D. (1981). Cell-substrate contacts illuminated by total internal reflection fluorescence. *Journal of Cell Biology, 89*(1), 141−145. http://dx.doi.org/10.1083/jcb.89.1.141.

Block, S. M., Goldstein, L. S. B., & Schnapp, B. J. (1990). Bead movement by single kinesin molecules studied with optical tweezers. *Nature, 348*(6299), 348−352. http://dx.doi.org/10.1038/348348a0.

Coelho, M., Maghelli, N., & Tolić-Nørrelykke, I. M. (2013). Single-molecule imaging in vivo: the dancing building blocks of the cell. *Integrative Biology, 5*(5), 748−758. http://dx.doi.org/10.1039/C3IB40018B.

Forsburg, S. L., & Rhind, N. (2006). Basic methods for fission yeast. *Yeast, 23*, 173−183. http://dx.doi.org/10.1002/yea.1347.

Gennerich, A., & Reck-Peterson, S. L. (2011). Probing the force generation and stepping behavior of cytoplasmic Dynein. *Methods in Molecular Biology, 783*, 63−80. http://dx.doi.org/10.1007/978-1-61779-282-3_4 (Clifton, N.J.).

Iino, R., Koyama, I., & Kusumi, A. (2001). Single molecule imaging of green fluorescent proteins in living cells: E-cadherin forms oligomers on the free cell surface. *Biophysical Journal, 80*(6), 2667−2677. http://dx.doi.org/10.1016/S0006-3495(01)76236-4.

Jaqaman, K., Loerke, D., Mettlen, M., Kuwata, H., Grinstein, S., Schmid, S. L., et al. (2008). Robust single-particle tracking in live-cell time-lapse sequences. *Nature Methods, 5*(8), 695−702. http://dx.doi.org/10.1038/nmeth.1237.

Kardon, J. R., & Vale, R. D. (2009). Regulators of the cytoplasmic dynein motor. nature reviews. *Molecular Cell Biology, 10*(12), 854−865. http://dx.doi.org/10.1038/nrm2804.

Kerssemakers, J. W., Munteanu, E. L., Laan, L., Noetzel, T. L., Janson, M. E., & Dogterom, M. (2006). Assembly dynamics of microtubules at molecular resolution. *Nature, 442*, 709−712. http://dx.doi.org/10.1038/nature04928.

Korten, T., Nitzsche, B., Gell, C., Ruhnow, F., Leduc, C., & Diez, S. (2011). Fluorescence imaging of single Kinesin motors on immobilized microtubules. *Methods in Molecular Biology, 783*, 121−137. http://dx.doi.org/10.1007/978-1-61779-282-3_7.

Krull, A., Steinborn, A., Ananthanarayanan, V., Ramunno-Johnson, D., Petersohn, U., & Tolić-Nørrelykke, I. M. (2014). A divide and conquer strategy for the maximum likelihood localization of low intensity objects. *Optics Express, 22*(1), 210. http://dx.doi.org/10.1364/OE.22.000210.

Kuo, S. C., & Sheetz, M. P. (1993). Force of single kinesin molecules measured with optical tweezers. *Science, 260*(5105), 232−234. http://dx.doi.org/10.1126/science.8469975.

Reck-Peterson, S. L., Derr, N. D., & Stuurman, N. (2010). Imaging single molecules using total internal reflection fluorescence microscopy (TIRFM). *Cold Spring Harbor Protocols, 2010*(3). http://dx.doi.org/10.1101/pdb.top73.

Reck-Peterson, S. L., Yildiz, A., Carter, A. P., Gennerich, A., Zhang, N., & Vale, R. D. (2006). Single-molecule analysis of dynein processivity and stepping behavior. *Cell, 126*, 335−348. http://dx.doi.org/10.1016/j.cell.2006.05.046.

Saito, T. T., Okuzaki, D., & Nojima, H. (2006). Mcp5, a meiotic cell cortex protein, is required for nuclear movement mediated by dynein and microtubules in fission yeast. *Journal of Cell Biology, 173*, 27−33. http://dx.doi.org/10.1083/jcb.200512129.

Sellers, J. (2000). Myosins: a diverse superfamily. *Biochimica et Biophysica Acta*, 3−22. http://dx.doi.org/10.1016/S0167-4889(00)00005-7.

Svoboda, K., Schmidt, C. F., Schnapp, B. J., & Block, S. M. (1993). Direct observation of kinesin stepping by optical trapping interferometry. *Nature, 365*(6448), 721−727. http://dx.doi.org/10.1038/365721a0.

Tokunaga, M., Imamoto, N., & Sakata-Sogawa, K. (2008). Highly inclined thin illumination enables clear single-molecule imaging in cells. *Nature Methods, 5*, 159−161. http://dx.doi.org/10.1038/nmeth1171.

Ulbrich, M. H., & Isacoff, E. Y. (2007). Subunit counting in membrane-bound proteins. *Nature Methods, 4*(4), 319−321. http://dx.doi.org/10.1038/nmeth1024.

Vale, R. D. (2003). The molecular motor toolbox for intracellular transport. *Cell, 112*(4), 467−480. http://dx.doi.org/10.1016/S0092-8674(03)00111-9.

Vale, R. D., Funatsu, T., Pierce, D. W., Romberg, L., Harada, Y., & Yanagida, T. (1996). Direct observation of single kinesin molecules moving along microtubules. *Nature, 380*(6573), 451−453. http://dx.doi.org/10.1038/380451a0.

Vale, R. D., Schnapp, B. J., Reese, T. S., & Sheetz, M. P. (1985). Organelle, bead, and microtubule translocations promoted by soluble factors from the squid giant axon. *Cell, 40*(3), 559−569. http://dx.doi.org/10.1016/0092-8674(85)90204-1.

Vogel, S. K., Pavin, N., Maghelli, N., Julicher, F., & Tolić-Nørrelykke, I. M. (2009). Self-organization of dynein motors generates meiotic nuclear oscillations. *PLoS Biology, 7*(4), e1000087. http://dx.doi.org/10.1371/journal.pbio.1000087.

Yamamoto, A., Tsutsumi, C., Kojima, H., Oiwa, K., & Hiraoka, Y. (2001). Dynamic behavior of microtubules during dynein-dependent nuclear migrations of meiotic prophase in fission yeast. *Molecular Biology of the Cell, 12*, 3933−3946. http://dx.doi.org/10.1091/mbc.12.12.3933.

Yamamoto, A., West, R. R., McIntosh, J. R., & Hiraoka, Y. (1999). A cytoplasmic dynein heavy chain is required for oscillatory nuclear movement of meiotic prophase and efficient meiotic recombination in fission yeast. *Journal of Cell Biology, 145*, 1233−1249. http://dx.doi.org/10.1083/jcb.145.6.1233.

Yamashita, A., & Yamamoto, M. (2006). Fission yeast Num1p is a cortical factor anchoring dynein and is essential for the horse-tail nuclear movement during meiotic prophase. *Genetics, 173*, 1187−1196. http://dx.doi.org/10.1534/genetics.105.050062.